



The effect of tree mortality on CO₂ fluxes in an old-growth spruce forest

D. V. Kareljin¹ · D. G. Zamolodchikov² · A. V. Shilkin³ · S. Yu. Popov⁴ · A. S. Kumanyaev² · V. O. Lopes de Gerenuy⁵ · N. O. Tel'nova¹ · Michael L. Gitarskiy⁶

Received: 23 March 2020 / Revised: 17 October 2020 / Accepted: 26 October 2020
© Springer-Verlag GmbH Germany, part of Springer Nature 2020

Abstract

Long-term (2009–2019) field studies of the CO₂ fluxes over the Valday upland in north-western European Russia were performed in an old-growth spruce-dominated forest subject to the combined effects of climate change, bark beetle attacks and windfall events. The annual carbon uptake within the study area decreased from $-300 \text{ g C m}^{-2} \text{ yr}^{-1}$ in 2010–2011 to $-95 \text{ g C m}^{-2} \text{ yr}^{-1}$ in 2018 as a result of progressive tree mortality. However, mortality did not cause a significant reduction in specific ecosystem respiration. The respiration of the damaged forest was formed by efflux from soil (64.8%), living vegetation (15.5%), hotspots under dry standing trees (12.1%) and decomposition of woody debris (7.6%). High correlations between net ecosystem exchange and dry standing spruce stocks and average soil CO₂ efflux were found. The decrease in the carbon sink was followed by a decline in evapotranspiration from $0.0142 \pm 0.0003 \text{ g H}_2\text{O m}^{-2} \text{ s}^{-1}$ for May–October 2010 to $0.0116 \pm 0.0002 \text{ g H}_2\text{O m}^{-2} \text{ s}^{-1}$ in 2018. We assumed that the decrease in carbon uptake was due to both the reduction in primary tree production and the decrease in the area of the unaffected stands. Our estimates show that an increase in tree mortality up to 27% of a stand area could turn an old-growth spruce forest into a net source of CO₂. This should be taken into account when considering human-induced and climate-related effects on boreal forests.

Keywords Soil respiration · Evapotranspiration · Net carbon flux · Debris decay · CO₂ hotspots

Communicated by Rüdiger Grote.

Electronic supplementary material The online version of this article (<https://doi.org/10.1007/s10342-020-01330-3>) contains supplementary material, which is available to authorized users.

✉ Michael L. Gitarskiy
m.gitarskiy@gmail.com

¹ Institute of Geography of the Russian Academy of Sciences (RAS), 29 Staromonetniy lane, Moscow, Russia 119017

² Center for Forest Ecology and Productivity RAS, 84/32 Profsoyuznaya Str., Moscow, Russia 117234

³ Tayphoon” Research Association of the Roshydromet, 4 Pobeda Str., Obrinsk, Kaluga Region, Russia 249038

⁴ Biology Department, Lomonosov State University, 1–12 Leninskie Gory, Moscow, Russia 119991

⁵ Institute for Physical, Chemical and Biological Problems of Soil Science RAS, Puschino-na-Oke, Moscow Region, Russia 142290

⁶ Dubna State University, Ugresha Branch, 24 Academician Zhukov Str., Dzerzhinsky, Moscow Region, Russia 140090

Introduction

Despite progressing human interference, forests remain the dominant terrestrial ecosystems that are highly important to the key climate stability factors ground albedo and atmospheric composition (Bonan 2008). Tree stands are the primary drivers of the organic matter cycle. Consequently, climate-related and human-induced changes in tree-stand vitality directly affect the carbon budget of forest ecosystems. The effects of forest damage on surface–atmosphere gas exchange have become of interest in the past two decades of intensive global temperature increases (Valentini et al. 2000; Bonan 2008; Lindroth et al. 2009; Köster et al. 2011; Peters et al. 2013; Štursova et al. 2014; Dobor et al. 2018; Ney et al. 2019, etc.).

Boreal forests comprise almost 14.9% of the global forest stock (Pan et al. 2013), and a majority of studies have focused on boreal conifers of North America and Europe. Being highly vulnerable, they have been damaged and been replaced by deciduous species (Allen et al. 2010). In the first years of disturbance, a boreal forest ecosystem rapidly

transforms into a net source of carbon dioxide (CO_2) due to decrease in growing stock. However, as secondary succession emerges, CO_2 removal increases again, finally offsetting emissions, and the ecosystem gradually recovers to a net sink (Dobor et al. 2018).

CO_2 emissions from soil are a key component of terrestrial respiration, and external disturbances are particularly important (Valentini et al. 2000; Bond-Lamberty and Thompson 2010). Despite the temporal variability, an instantaneous CO_2 release from a specific location remains relatively similar from year to year since it is mostly determined by conventional soil properties (Karelin et al. 2014). The general and specific C balances in soil are affected by the replacement of primary forest communities with secondary communities and then affected by age, size and tree species changes that are frequently a result of natural and human-induced destruction (Weibin et al. 2017; Han et al. 2018; Shu et al. 2019). Destruction of forests can occur due to (i) air pollution (Koptskik et al. 2015), (ii) clear-cuts (Köster et al. 2011; Williams et al. 2014; Kohout et al. 2018; Ney et al. 2019; Mamkin et al. 2019), (iii) forest fires (Martínez-García et al. 2015), (iv) pest outbreaks (Frank et al. 2014; Hicke et al. 2012; Štursová et al. 2014), (v) windfall events (Knöhl et al. 2002; Lindroth et al. 2009; Lindauer et al. 2014; Knoch et al. 2015; Matthews et al. 2015) and eventually climate change (Dobor et al. 2018; Curiel Yuste et al. 2019), which may even exacerbate the impacts of the factors from (iii) to (v). Finally, these factors increase ecosystem respiration (hereafter referred to as *ER*) and, in particular, CO_2 emissions from soil.

There are frequent cases of “hotspots” with abnormally high CO_2 emissions from forest floors that are more than an order of magnitude above background respiration and thus introduce high uncertainty into microscale projections (Martínez-García et al. 2015). The hotspots differ from rapidly decreasing gas release events such as the wind-regulated pumping effect (Baldocchi and Meyers 1991; Subke et al. 2003), molecular desorption from mechanical damage (i.e. falling large tree stems (Karelin et al. 2017a) and soil layer destruction (Smagin et al. 2016) and the effect of radiative forcing. Continued CO_2 release to the atmosphere occurs through dry stumps (Martínez-García et al. 2015) and under dead trees over post-fire sites (Curiel Yuste et al. 2019). Hotspot intensity depends on fine-root density, organic matter reserves, litter stocks, soil moisture, bulk density and soil water pH (Fang et al. 1998; Morris 1999; Xu and Qi 2001; Qi et al. 2010; Karelin, et al. 2014; Martínez-García et al. 2015, etc.). Soil properties control the rate of CO_2 production by roots and microbiota and CO_2 transport and subsequent release to the atmosphere. Thus, soil temperature, porosity and burrowing animals increase CO_2 intensity, whereas pH is important for gas transport and storage (Smagin 2005). CO_2 transport is highly important in heavy

soils such as wetland soil (Bohn et al. 2013), while biogenic factors are the major contributors to emissions from low-productivity soils such as sands and soil in industrial areas (Koptskik et al. 2015). Hence, CO_2 intensity in forest ecosystems is regulated by specific drivers whose properties are not yet well understood. In addition, it is worth assessing carbon balance variability in terms of stand vitality decline. The aim of our study was to trace the changes in CO_2 and water budgets during the long-term (2009–2019) transformation of a boreal spruce forest from an undisturbed state to progressive decay. The following specific studies were performed:

- (i) Assessed net carbon balance changes;
- (ii) Estimated the input of hotspots to gross respiration and net CO_2 balance;
- (iii) Determined the role of bacteria and xylotrophic fungi in hotspot formation and CO_2 release;
- (iv) Verified the hypothesis on the positive link between the net carbon balance and the proportion of dry trees in a stand; and
- (v) Used the 2010 and 2018 evapotranspiration rates to test the assumption that bark beetle attacks reduce the photosynthetic activity of spruces, which could result in their dieback (Frank et al. 2014).

Objects and methods

Study area

Our study builds upon the continuous monitoring of the overmature spruce forest of the “Taiga Log” experimental site, Valday branch of the State Hydrological Institute of the Roshydromet (Valday region, Novgorod oblast, Russian Federation, N57°57'43.0", E33°20'19.4", 225.8 m above sea level; Fig. 1). The site is equipped with 45-m high durable metal towers that are used for eddy covariance measurements and are described in Section “Eddy covariance measurements”. The monitoring started in 2009 and is currently ongoing. The forest initially was 90% spruce trees and 10% pine trees, with an average diameter of 37 cm at a 1.3 m height (hereafter referred to as the diameter at breast height, dbh) and an average height of 31 m. The forest had a density of 0.6 and the highest quality class of I. The understory had a density of 0.3 with the predominance of spruce (*Picea abies* (L.) H. Karst.) and rowan (*Sorbus aucuparia* L.). Herbs and shrubs covered 70% of the ground dominated by the boreal species *Calamagrostis arundinacea* (L.) Roth., *Maianthemum bifolium* (L.) FW Schmidt and *Oxalis acetosella* L. The combination of boreal (*Vaccinium myrtillus* L., *V. vitis-idaea* L., *Luzula pilosa* (L.) Willd., *Trientalis europaea* L.) and nemoral (*Lamium galeobdolon* (L.) Krantz, *Aegopodium podagraria* L. and *Stellaria holostea* L.) species was typical

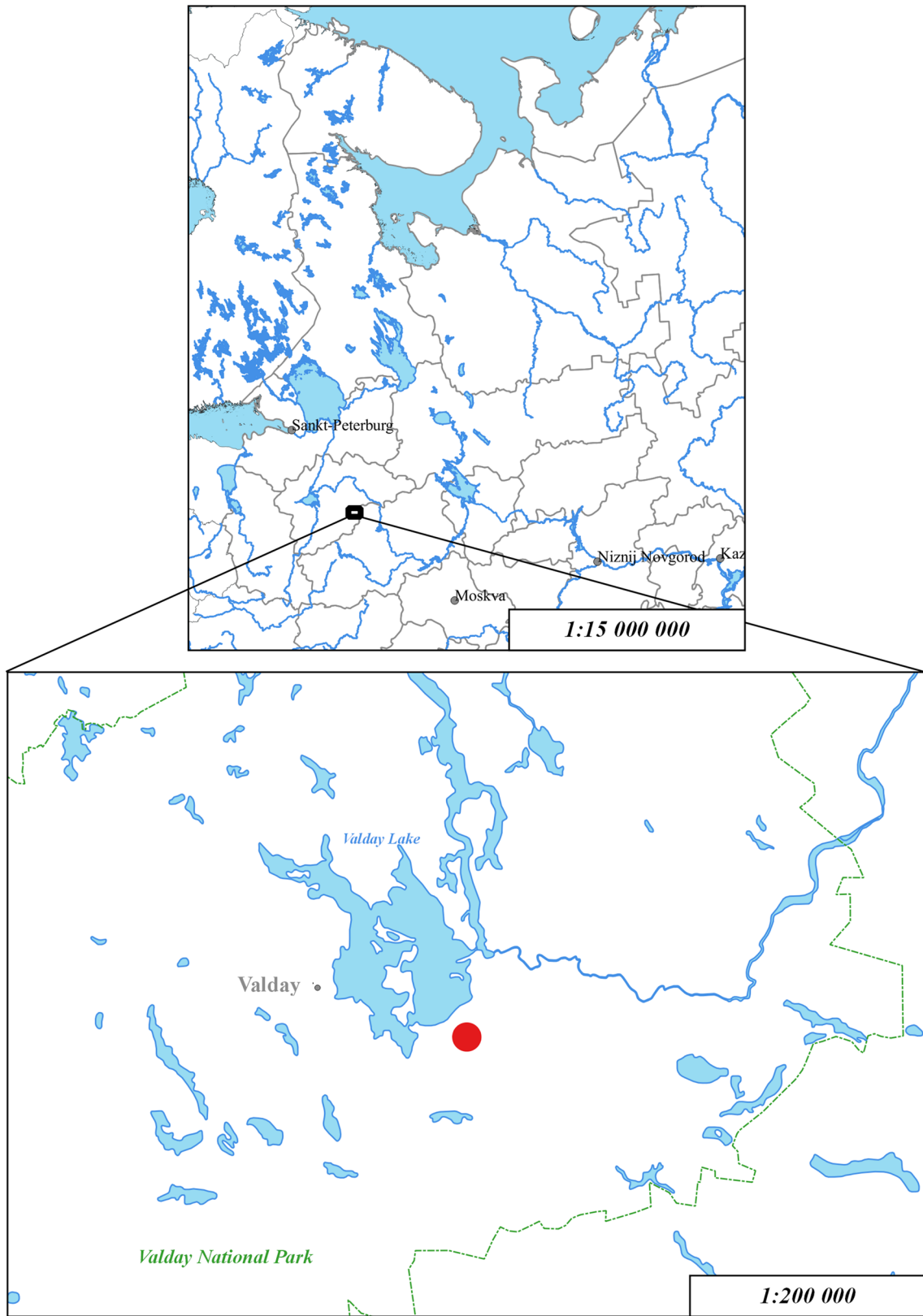


Fig. 1 Location of the study area. The red circle represents the *EC* footprint

for ground vegetation. Green mosses (*Pleurozium schreberi* (Brid.) Mitt., *Hylocomium splendens* (Hedw.) Schimp. and *Dicranum* sp.) dominated in the moss layer, cover of 70% of the area.

The study area also included open spaces that emerged from windfall events. Apart from a few living trees, they contained dry standing trees, windfall trees and stumps of Norway spruce from 3 to 30 m in height (length for windfall) and 31 to 50 cm in diameter. The tree canopy was totally destroyed, and undergrowth reached a height of 4.5 m and a density of 0.4. The rowan trees were dominant, but the share of *Salix caprea* L. was also substantial. The mid-summer cover of herbs and shrubs was almost 100% dominated by *Rubus idaeus* L., *Pteridium aquilinum* (L.) Kuhn., *Dryopteris dilatata* (Hoffm.) A. Gray and *S. nemorum* L. that formed the undergrow that 1 to 1.5 m in height.

From 2010 to 2014, the stand sharply declined as a result of extreme drought (2010) and subsequently combined insect (bark beetle *Ips typographus* L.) and fungi (mottled butt rot) attack. A similar phenomenon occurred in the Czech Republic, where a spruce forest was destroyed by bark beetles, and dead roots decomposed by white rot soil saprotrophic fungi became CO₂ “hotspots” two years after felling (Štursová et al. 2014; Kohout et al. 2018). We hypothesized that xylotrophic fungi simultaneously attacked both the aboveground and belowground parts of the dry standing trees, including their stem base, and the decomposition rates of both parts were the same. The red belt fungus (*Fomitopsis pinicola* Karst.), the most common boreal xylotrophic fungi that cause brown rot, was used as the damage indicator.

Relief and soils

The current terrain and surface sediments of the “Taiga Log” site formed mainly as a result of Valday glaciation. The area has a diverse lithological composition represented by terminal moraine ridges and inter-ridge depressions. In 2012–2018, DE Konyushkov undertook soil studies of the site that involved the assessment of 35 soil pits (Alferov et al. 2017). The local soils are Stagnic Albic Podzol (Arenic, Ruptic) with varying degrees of erosion and Albic Podzol (Ruptic). Their upper layer has a loamy sand to sand texture and is underlain by loam and less often underlain by clay or the coarse sand with pebbles. The layers containing carbonate material are usually found at depths ranging from 80–100 cm to 2–3 m. The soils of inter-ridge depressions are mainly Stagnic Albic Podzols (Arenic and Ruptic) and Histosols. The litter usually consists of fresh and poorly decomposed debris from moss, spruce needles and small twigs. It is moist and has the greenish brown colour. The sub-litter humus layer on the moraine ridges frequently emerges as the former arable layer (the most elevated ridges were ploughed until the nineteenth century) marked with a dark grey colour

with the presence of microcharcoal particles. The mixed-grained sandy layer with numerous gravel-size clasts and small boulders increases with depth and occurs in the lower part of the soil profile. The bulk organic carbon content in the litter, topsoil (humic) and mineral subsoil horizons of the automorphic soils was estimated as 80 t ha⁻¹. In semi-hydromorphic soils, this value increases to 138 t ha⁻¹, and in peatlands, it increases to 1200–1600 t ha⁻¹. Based on its relative occurrence (80:10:10%), the soil organic carbon pool of the experimental site was estimated to be 200 to 240 t ha⁻¹ (Alferov et al. 2017).

Local climate and weather conditions

The weather and climate data were provided by the Valday branch weather station at the State Hydrological Institute. The local climate is humid with surplus rainfall. The mean annual temperature for 2009–2019 was 5.2 ± 0.19 °C, which was significantly higher than the climatic normal of 4.0 °C for 1961–1990 (one sample t test, $p < 0.0001$).¹ The mean annual precipitation for the same period (2009–2019) was 830.1 ± 35.6 mm, which was also higher than the normal value of 723 mm (one sample t test, $p = 0.021$). The differences in the temperature and precipitation from the 1931–1960 climatic normal values were even more pronounced ($p < 0.0001$ and $p = 0.014$, respectively). However, the annual hydrothermal regime did not change because the increase in incoming heat was compensated by the enhanced precipitation. Therefore, although Selyaninov’s hydrothermal coefficients have not significantly changed (1.75 ± 0.13 for 2009–2019 and 1.78 for 1961–1990; one sample t test, $p = 0.83$),² the environmental conditions became warmer and more humid during the 10-year period of the study, which could have affected the local growth conditions of the spruce stand.

Study area interpretation, satellite data, geobotanical analysis and the assessment of standing stock and coarse woody debris

Our studies covered the area around the tower with the installed eddy covariance hardware. Following the general assumptions for the eddy covariance method (Burba 2013), the maximum radius of the site was estimated 500 m. Thus, it formed a circle that was 1 km in diameter and an area of

¹ The climatic normal was calculated from the weather data from the Valday branch of the State Hydrological Institute.

² The Selyaninov’s hydro-thermal coefficient (HTC) is calculated as: $HTC = \Sigma P / 0.1 \Sigma H$, where ΣP is the total precipitation (mm) for the period with temperatures above +10 °C, and ΣH is the sum of the diurnal temperatures above +10 °C for the same timeframe (Selyaninov 1928). The HTC informs the water availability determination.

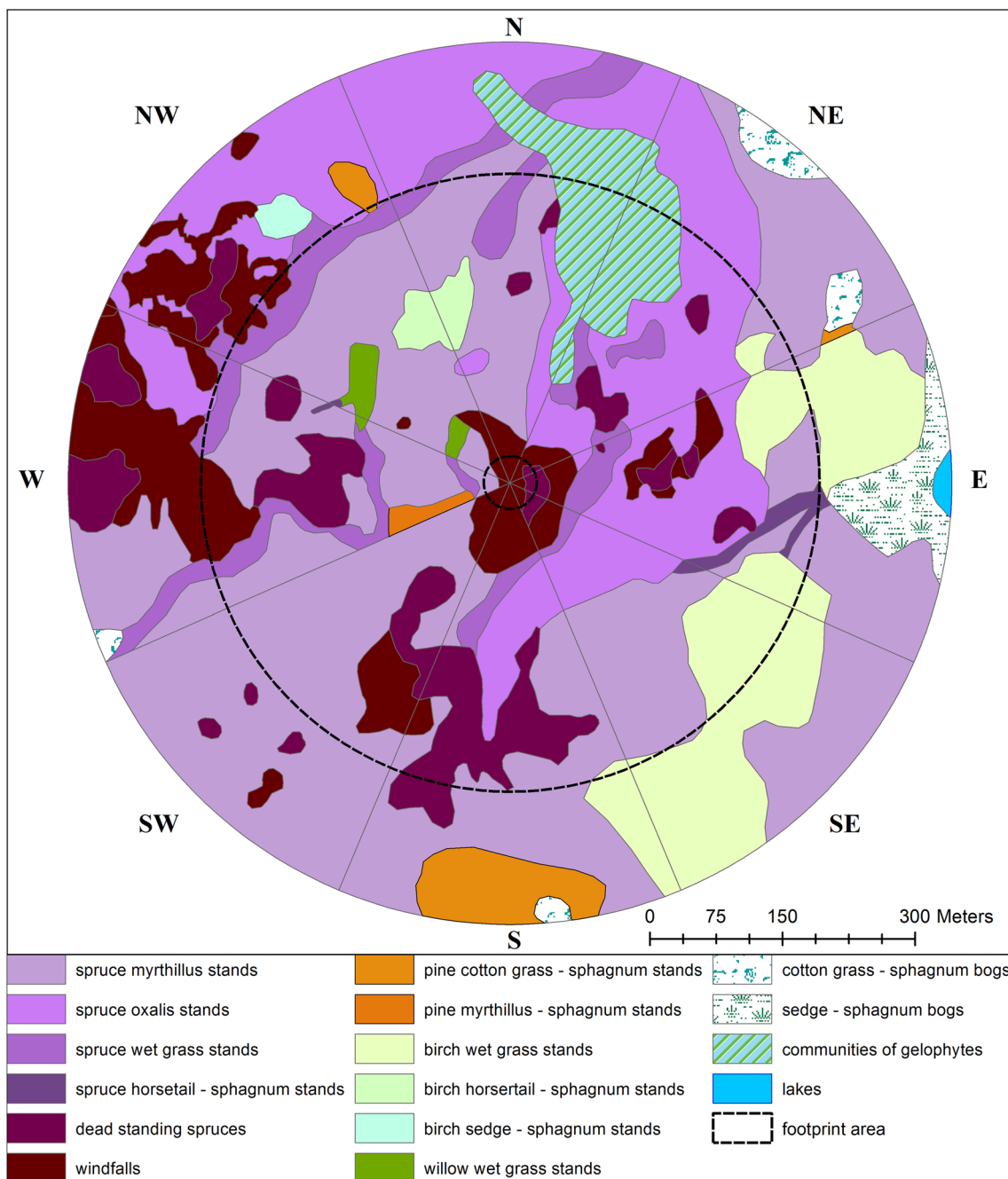


Fig. 2 The map of the major forest biotopes across the cone-shaped sectors of the *EC* footprint

approximately 0.785 km², which is referred to as an *EC* footprint. The *EC* footprint was subdivided into eight 45° cone-shaped sectors. The proportions of the major biotopes were estimated for each sector and attributed to a 0.5-h average net CO₂ eddy flux for the periods when the wind direction was within it. The assessments were conducted from May to October of 2010 and 2018, and from April to July of 2019, comprising 6475, 7677 and 5306 half-hour eddy flux measurements, respectively. Vegetation mapping, geobotanical

descriptions and carbon stock estimates of aboveground biomass, dead standing trees and coarse woody debris were performed inside the footprint in 2018 and 2019.

The vegetation mapping was performed with 3-band red, green and blue (RGB) composite *GeoEye* satellite images obtained in 2018 (UTM projection zone 36, WGS 84, resolution 0.5 m per 1 pixel). Based on the 92 circular sample plots, each with a 25-m radius, the footprint was subdivided into polygons with different plant communities (Fig. 2).

The geobotanical inventory included the identification of plant species and assessment of their cover and distribution following the method of Zaugolnova (2002). The polygons were subsequently digitized with ArcGis 10.0 software (ESRI CIS Ltd. version 2012, <https://www.esri-cis.ru/>).

Height, dbh and vitality were estimated for each living tree, undergrowth and understory species over the 25 × 40-m permanent plot that was established inside the footprint in 2009. The measurements were used for calculation of above-ground phytomass (m^3ha^{-1}) and carbon (td. m. ha^{-1}) stocks. The calculations were performed with the use of allometric equations and conversion factors developed by Utkin and elaborated by Korotkov (Utkin et al. 1996, 2005; Alferov et al. 2017).

The dry standing trees were assessed in the 92 circular sample plots. Their volume stock (m^3ha^{-1}) was calculated based on the height and dbh measurements with allometric equations and conversion parameters (Utkin et al. 1996, 2005; Alferov et al. 2017). Decomposition degree was assessed following Treifeld's 5-stage decay scale (Treifeld et al. 2002). Carbon stock (td. m. ha^{-1}) was calculated from the volume stock with the use of conversion factors disaggregated by tree species and decomposition degree (Utkin et al. 1996; Zamolodchikov et al. 2005).

The coarse woody debris storage was estimated following the method by Warren and Olsen (1964) modified by Grabovskiy and Zamolodchikov (2012). The data were collected along the 50-m-linear transects laid throughout the studied ecosystems. The data consisted of the identification of species and decomposition stage, the measurements of top and bottom diameters and the entire length of each debris fragment with a > 2-cm diameter that were found at the intersection with the transect. Decomposition was assessed based on Treifeld's scale (Treifeld et al. 2002). The carbon stocks in the coarse woody debris per area unit (td. m. ha^{-1}), volume (m^3ha^{-1}) and surface (m^2ha^{-1}) disaggregated by tree type and decomposition degree were calculated with the use of the software tool of VI Grabovskiy (<https://cepl.rssi.ru/r-and-d-8/>). Then, the total surface area of coarse woody debris disaggregated by species type and decomposition degree was calculated for the major biotopes of the footprint.

Eddy covariance measurements

The CO_2 and water vapour (H_2O) fluxes were measured with the eddy covariance (EC) method. The principal EC hardware included a CR500 data logger (Campbell Scientific Inc., USA), CSAT-3 sonic anemometer (Campbell Scientific Inc., USA) and LI-7500 infrared $\text{CO}_2/\text{H}_2\text{O}$ open path analyser (LI-COR Inc., USA). They were installed at a 38-m height on the well-grounded 45-m metal tower, where the spruce forest had a maximum canopy height of 32 m. The EC hardware included 3 HFP01 soil heat flux sensors (Hukseflux

Thermal Sensors, the Netherlands), at 8 cm underground; 2 TCAV soil temperature sensors (Campbell Sci. Inc., USA), at 2–6 cm underground; and 2 CS616 reflectometers (Campbell Sci. Inc., USA), at 2.5 cm underground. All soil sensors were located within 1 m of the tower. The weather data were assessed with 5 T107C air temperature sensors (Campbell Sci. Inc., USA) installed at heights of 2.0, 8.5, 17.5, 26.5 and 35.5 m; the HMP45C air temperature and moisture sensor (Vaisala Inc., Finland), at 38 m above ground; the NR-Lite net heat radiometer (Kipp & Zonen B.V., the Netherlands), at 42 m aboveground; the LI190SB photosynthetically active radiation metre (LI-COR Inc., USA), at 42 m aboveground; and the TE525 precipitation register (Campbell Sci. Inc., USA), at 42 m aboveground. Together with the CR500 data logger, CSAT-3 sonic anemometer and LI-7500 infrared $\text{CO}_2/\text{H}_2\text{O}$ analyser, the sensors were integrated in the Open Path Eddy Covariance (OPEC) system (Campbell Sci. Inc., USA). The OPEC system was continuously operating from 2010 to 2011. From 2011 to 2015, the observations were interrupted because of lightning damage. After 2015, the hardware was restored and the observations continued.

In 2017, the OPEC was supplemented with the CPEC-200 Close Path Eddy Covariance system (Campbell Scientific, USA). The CPEC200 hardware was installed on the same tower at a height of 42 m and included the EC155 infrared $\text{CO}_2/\text{H}_2\text{O}$ close path analyser, the CSAT3A 3-D sonic anemometer, the EC100 controller, a pump, a seat valve and the CR3000 data logger. The EC155 analyser operation entailed continuous pumping through the closed optic channel of the sample air followed by its 10-Hz frequency-modulated spectral infrared analysis. The hardware underwent daily automatic calibration with WMO gas standards and high-purity nitrogen. Since 2017, open and close path EC measurements occurred in parallel enabling their comparison and verification.

The CO_2 and H_2O vertical distribution in the 0–42-m air profile was assessed with the AP200 Atmospheric Profile system (Campbell Sci. Inc., USA) installed 12 m aboveground of another well-grounded 45-m metal tower 50 m away. The profile concentrations were alternately measured at the 8 height levels (0.25, 1.0, 2.0, 8.5, 17.5, 26.5, 35.5 and 40.0 m). Air sampling was performed through a preheated 750-ml intake assembly, where the air was mixed to correct concentration fluctuations. From the intake assembly, the air went through aluminium-reinforced polyethylene tubes and the built-in 11-valve operator to the Li-840A infrared $\text{CO}_2/\text{H}_2\text{O}$ close path analyser (LI-COR Inc., USA). The system was operated by the CR1000 datalogger (Campbell Sci. Inc., USA) that accumulated measurement data and controlled automatic daily calibration with WMO gas standards and high-purity nitrogen.

The EC data were downloaded from the dataloggers and archived. The archive includes concentration, atmospheric



Fig. 3 The site with spruce damage in the Valday forest (photograph by DV Karelina, May 2015). Circles denote the areas under the standing dry trees with increased CO_2 release (hotspots)

pressure, wind speed, moisture and temperature measurements for the entire period of the observations. It also includes high-frequency data (10 Hz) that were used for the calculation of CO_2 , H_2O and heat fluxes. The details of the 2 EC systems operations, filter and gap-filling procedures and data quality assessment are provided in Supplementary Materials for the manuscript.

The EC fluxes were calculated from the raw data for 30-min time intervals using EddyPro software (*LI-COR Biosciences, USA*), which also conducts statistical tests and corrections. The data processing was performed with the use of conventional methods (Burba 2013). The net ecosystem CO_2 and H_2O flux measurements were combined with simultaneous CO_2 measurements from the soil, ground vegetation and coarse woody debris as described below.

Measurements of CO_2 soil efflux

The spatial variability in CO_2 soil efflux (herewith also referred as soil respiration) was assessed along the 490-m transect in the east-to-west direction through all major biotopes of the footprint across three moraine ridges and inter-ridge depressions. The effect of tree mortality on the small CO_2 flux and carbon budget was analysed over a 15×15 -m

permanent plot set inside the footprint at the edge of spruce forest and an open space that formed from the windfall events in 2011–2012 and expanded from 0.5 to 1 ha over the next 5 years (Figs. 2, 3).

Soil respiration was assessed by the closed chamber method. Opaque PVC 1.2–1.5-L cylindrical chambers with an area of 90 cm^2 were inserted into the soil at a depth of 2–3-cm without surface vegetation inside. In total, 50 permanent chambers were uniformly installed along the 490-m transect, crossing all major forest biotopes and relief elements. The other 20 chambers were set over the 15×15 -m plot for hotspot efflux measurements: 10 chambers were set 10 to 20 cm apart from the stems of dry standing trees, and the other 10 were set in the inter-stem locations, 2–6 m from dry stems. After installation, all chambers were kept open for at least 24 h before the measurements. During the measurements, they were closed with a hermetic lid with a built-in 4×4 -cm 12-V fan. The lid was connected with a gas analyser through polyethylene tubes. Each measurement started after a 30-s delay and lasted for 1–3 min depending on the efflux intensity. The chambers were temporarily removed from the soil in December–March.

The CO_2 was measured with *LiCor 6200*, *LiCor 6400* and *LiCor 8100A* portable infrared analysers (*LI-COR Inc.*,

USA). In addition, LI-COR 8100-102 and 8100-104 soil chambers (*LI-COR Inc.*, USA) were used to cross-check the results. The efflux rate was calculated with built-in software for the *LI-6200*, *LI-6400* and *LI-8100A* analysers (*LiCor Biosciences*, <https://www.licor.com/>) and corrected for the internal volume of the chambers. Soil respiration was measured along the transect monthly throughout the entire growth season (April–October 2013–2019). A 15 × 15-m plot was measured on the same dates in 2014–2018. In addition, the 24-h respiration measurements in the undamaged and decayed spruce biotopes were performed monthly in April–October 2013. The mean daily values showed nonsignificant differences from the daytime average data. Hence, the mean daytime-based respiration measurements were extrapolated to estimate seasonal and annual CO₂ soil effluxes. Winter respiration measurements were performed in January 2014 and February 2018. The 7-yr transect data set combined 1590 individual efflux measurements, and the 5-yr plot data set combined 480 individual efflux measurements.

Forest-floor flux measurements

The CO₂ forest-floor flux was assessed with 50 × 50 × 80-cm opaque chambers equipped with built-in fans. For the 1–3-min measurements, the chambers were positioned on the forest floor and hermetically sealed with water locks on 50 × 50-cm square aluminium bases installed at a 2–3-cm soil depth for the entire growing season. In addition, 2 opaque PVC chambers were put inside the bases that were free from vegetation for the soil respiration measurements. The measurements were performed every month from April to October 2018 over the windfall area (15 × 15-m plot) and in the spruce forest (25 × 40-m plot) at 10 locations for each. The respiration of the forest floor was estimated as the difference between the specific diurnal CO₂ fluxes with and without plants. The estimates were recalculated for the growing season with the trapezoidal method.

Laboratory measurements of soil microbial respiration

Cylindrical soil monoliths 10 cm in diameter and 15 cm in height were obtained from the topsoil layer near the permanent PVC chambers in a 15 × 15-m plot to assess the specific soil density and root content. The samples from the 2–15-cm soil layer were obtained near the dry standing spruces. The samples were obtained in a fivefold repetition pattern. The monoliths were analysed in the laboratory to determine the basal mineralization rate (V_{basal}), substrate-induced respiration (V_{sir}) and the mass of the soil microbial community (C_{mic}) following the method by Anderson and Domsch (1978). The metabolic coefficient (qCO₂) $V_{\text{basal}}/V_{\text{sir}}$ and

$V_{\text{basal}}/C_{\text{mic}}$ ratio were calculated from the results to assess the substrate availability for the microbial community (qCO₂) and microflora involvement in organic matter decomposition ($V_{\text{basal}}/C_{\text{mic}}$), respectively.

CO₂ emissions from coarse woody debris

The CO₂ emissions from the coarse woody debris were measured from April to October 2012–2017 by the closed chamber technique. The PVC opaque stationary chambers, 10 cm in diameter and 9–15 cm in height, were installed on lying and standing fragments of spruce debris with a diameter close to the average diameter of the stand. In total, 29 chambers were installed within the footprint. Prior to the measurements, the chambers were hermetically sealed with lids. Changes in the CO₂ concentration were measured for 3 min with a CO₂ portable analyser connected to the chambers with polyethylene tubes. The diurnal estimates were recalculated for the warm period and the calendar year (Gitarskiy et al. 2017, 2020). For periods with monthly air temperatures < 0 °C (November–March), the efflux from the coarse woody debris was assumed to be negligible. The measurements were accompanied by debris inventories based on Treifeld's decomposition scale (Treifeld et al. 2002; Safonov et al. 2012; Gitarskiy et al. 2017, 2020). The CO₂ surface effluxes from soil respiration and coarse woody debris were further extrapolated for the biotopes and the entire footprint. Furthermore, 555 measurements of CO₂ emissions from the coarse woody debris surface were performed from 2015 to 2017 for the forest biotope, and 365 CO₂ measurements were performed for the windfall area.

Assessment of dry stem wood decomposition

The wood cores were obtained in a threefold repetition pattern from each dry standing spruce stem over the 15 × 15-m plot at a height of 1.3 m with a 30-cm wood drill (*Haglof Forestry Instruments*, Sweden). The decomposition of the stem wood (DD) was estimated as a sum of the following variables:

$$\text{DD} = \text{WD} + \text{BR} + \text{FN} + \text{BRT} + \text{AG}, \quad (1)$$

where WD is the wood density estimated as a ratio of the number of solid core fragments to total core length, BR is the proportion of the bark lost (0–1), FN is the total number of live and dead bodies of bracket fungus on the stem, BRT is the presence of brown rot (0–3 points), and AG is the maximum age of bracket fungus bodies (years).

The indicators were chosen from preliminary field data and were based on a positive relationship with wood decomposition degree. Prior to summing, the indicators were standardized and transformed into scale points. The data

were rescaled with the MS Excel *STANDARDIZE* function to obtain a mean of zero and a standard deviation of 1. For each observed value of a given variable, the function subtracted the mean and divided it by the standard deviation. In the next step, to avoid negative numbers, the values were linearized:

$$y = a \times \left(\frac{x - \bar{X}}{S_x} \right) + b, \quad (2)$$

where x is the original value of the variable, y is the standardized value of the variable, \bar{X} is the average of the variables, S_x is the standard deviation, and a and b are the empirical parameters of the linearization (in our case $a=3$ and $b=6$).

After this procedure, the sums of values in all variables became equal.

Data treatment and modelling

The annual CO₂ emissions from under dry standing trees were calculated by trapezoidal interpolation of the measurements performed in 2014–2019. Regression modelling was applied to assess the contribution of the soil and dry standing trees to the annual CO₂ efflux from the 15 × 15-m plot. The seasonal and annual fluxes were estimated with a 3-h-step regression-based empirical model (Karelin et al. 2014). The weather data were obtained from the Valday weather station and the EC measurement database. For the periods with a positive mean daily air temperature (> 0 °C, warm period), the sum of the 4-day precipitation and 27-h air temperature records collected before soil emission measurements were used as the independent input variables. For the periods with negative daily air temperatures (< 0 °C, cold period), only air temperature was used as the independent input variable. The determination coefficients (r^2) were 0.656 for the warm periods and 0.747 for the cold periods ($p < 0.001$).

The annual forest carbon budget for 2013 was modelled as described in our manuscript (Alferov et al. 2017). In brief, the input data for this model were collected from the three 25 × 40-m monitoring plots that were set in 2013; two plots were in a living spruce forest, and one was in an area with only dead trees. The net ecosystem exchange (NEE) was calculated as the difference between the net primary production (NPP) and heterotrophic respiration. The NPP was derived as the change in the tree and shrub growing stock that was calculated by the method described in Section "Study area interpretation, satellite data, geobotanical analysis, and the assessment of standing stock and coarse woody debris". Heterotrophic respiration was obtained from the measurements in the opaque closed chambers (see Sections "Measurements of CO₂ soil efflux" and "CO₂ emissions from coarse woody debris"). Ecosystem respiration was estimated as a sum of the CO₂ fluxes from the soil, coarse woody debris and living

spruce stand. The respiration of the living spruce stand was assessed through intact shoot and stem chamber measurements at various heights (Alferov et al. 2017).

Calculations and statistical data treatment were performed with MS Excel and PRIMER V.7 (PRIMER-E Ltd.) software (Anderson et al. 2008). The nonparametric median test or Mann–Whitney *U* test was used to compare the average values at the significance level of $p = 0.05$. The mean values and their standard errors are given in the text; r_p denotes the Pearson correlation.

Results

Soil CO₂ efflux from the hotspots

The results demonstrated minor diurnal fluctuations in soil respiration intensity, so the mean daily and daytime average values differed but not significantly (Karelin et al. 2014). The CO₂ emissions smoothly increased in the biotopes with intensive spruce mortality regardless of inter-annual weather fluctuations. In 2014, the emissions were 16.5% above the soil efflux for the undestroyed stands measured in 2009–2010 and were used as the reference level. However, the emissions exceeded the reference level by 19% in 2017. During the warm periods (April–October), the average ratios between the CO₂ soil effluxes within a 0.5-m distance from the dry standing trees and in the inter-stem areas, used as the reference site, varied from 3.0 to 3.3 and were fairly stable to the inter-annual variations (Fig. 4). The only significant deviation (2.28) was detected in 2017. Apparently, the deviation was the result of increased soil moisture after intensive rainfall, and this scenario caused the dramatic decrease in emissions from the reference site and those under the dry standing trees (Fig. 5). In turn, the decrease in the ratio can be explained by the relationship with volumetric soil moisture (Fig. 6), which serves as the main driver for inter-annual variability in CO₂ soil effluxes in this forest type (Alferov et al. 2017). In general, a much stronger positive response of soil respiration to temperature increases and more negative response to soil moisture increases was observed under the dry standing spruces than under the inter-stem area (figs. 6 and 7). However, the effects of temperature on specific fluxes and the ratios between them were observed at an annual scale only, as seen from the data for all years (Fig. 8).

The analysis of the topsoil layer monoliths showed that soil density was significantly lower near the stems of the dry spruce trees ($0.31 < 0.74$ g cm⁻³, median test, $p = 0.046$) than in the other areas due to incorporation of woody debris fragments (in particular, bark). The density of the roots in the upper soil layer near the dry trees was also lower ($2.2 < 4.2$ kg m⁻³ median test, $p = 0.048$). These results indicate a relatively low contribution of root respiration.

Fig. 4 The changes in the soil CO_2 emission ratio for the areas under the dry spruce trees (-2-) and the background level in relation to the volumetric moisture in the 0–6-cm soil layer (-1-) for the period of observation. The average values and their standard errors are given

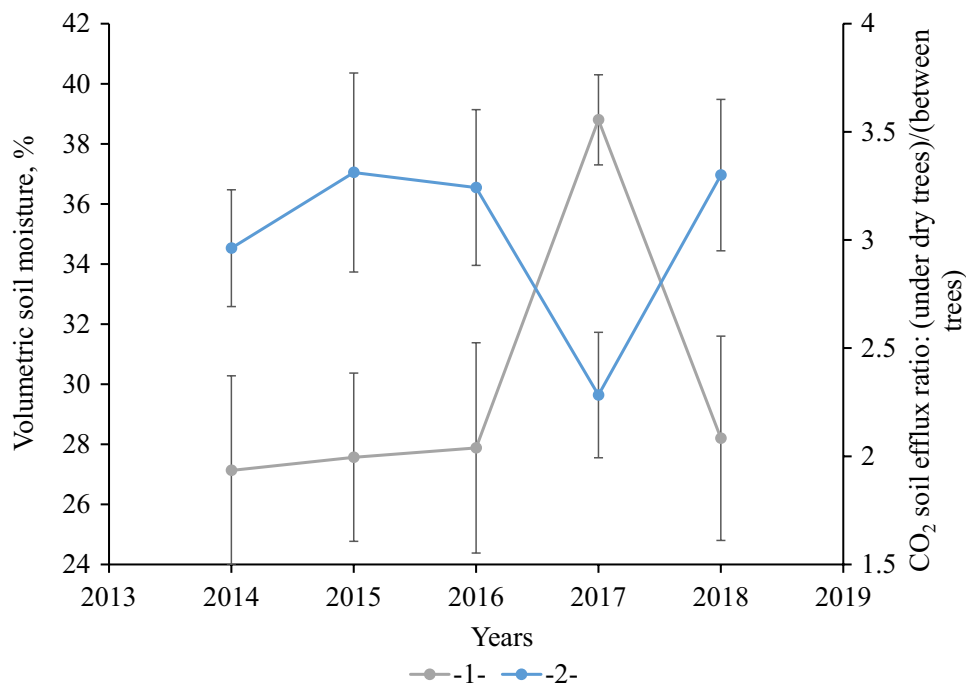
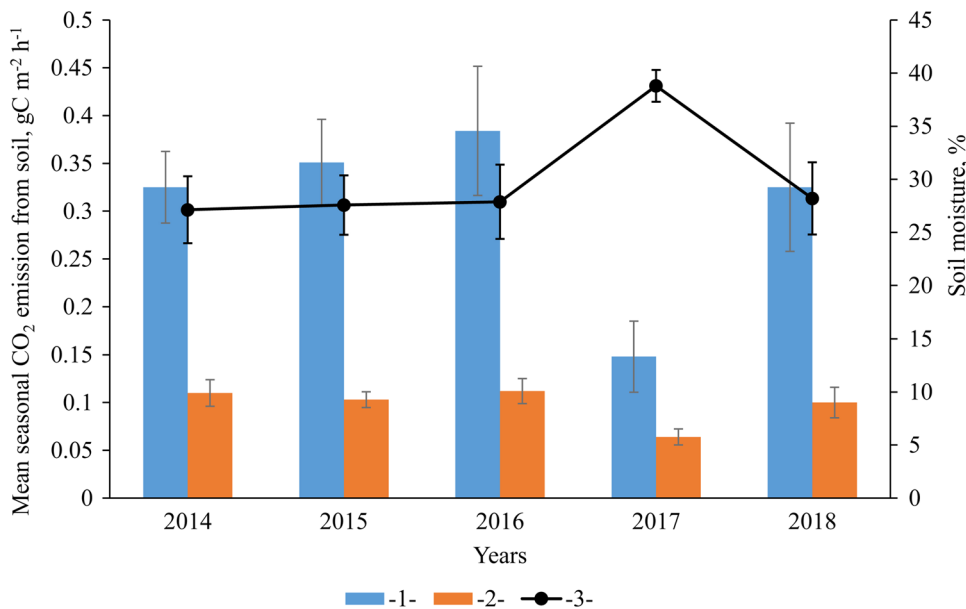


Fig. 5 The dynamics of the average CO_2 soil efflux rate for the snowless season (May–October) under the dry standing spruce stems and the stumps (-1-) and the background soil emission rate (-2-) vs. the volumetric soil moisture in the 0–6-cm soil layer (-3-). The average values and their standard errors are given



On the other hand, the April to October average soil temperature at the 10-cm depth was reliably lower ($8.9 < 9.4^\circ\text{C}$, Mann–Whitney test, $p=0.05$), and the volumetric humidity was higher ($32.4 > 28.9\%$, Mann–Whitney test, $p=0.04$) under the dry trees than in the inter-stem locations.

The basal mineralization rate and the mass of the soil microbial community determined in the upper soil layer were typical for a fairly suitable environment and sufficient nutrient resources. This result was confirmed by the absolute values of the $q\text{CO}_2$ parameter ranging from 0.320 to

0.421 with minor variance. The $V_{\text{basal}}/C_{\text{mic}}$ ratio showed the involvement of fungi, bacteria and other soil microorganisms in the decomposition process, which shows high microflora activity despite the nonsignificant difference in absolute values (from 0.042 to 0.055). The differences in these values between the closest to dry standing tree locations and the inter-stem areas were also identified. Substrate-induced respiration was higher under the dry standing trees ($2.05 > 1.17 \mu\text{g C per g soil } \text{h}^{-1}$, median test, $p=0.048$) than in the other areas, and there was also an increasing trend

Fig. 6 The relationship between the soil CO₂ efflux and the volumetric soil moisture in the 0–6-cm layer under the dry standing spruce trees and the stumps (-1-) and at the background sites (-2-) (“Taiga Log” experimental site, 2014–2018). The linear and quadratic regressions are given

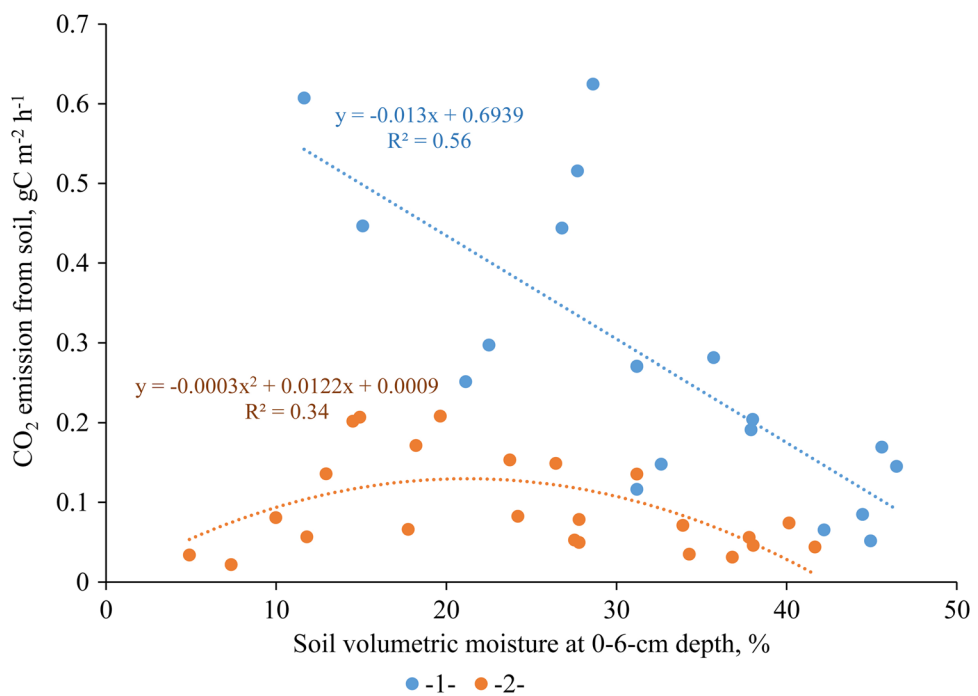
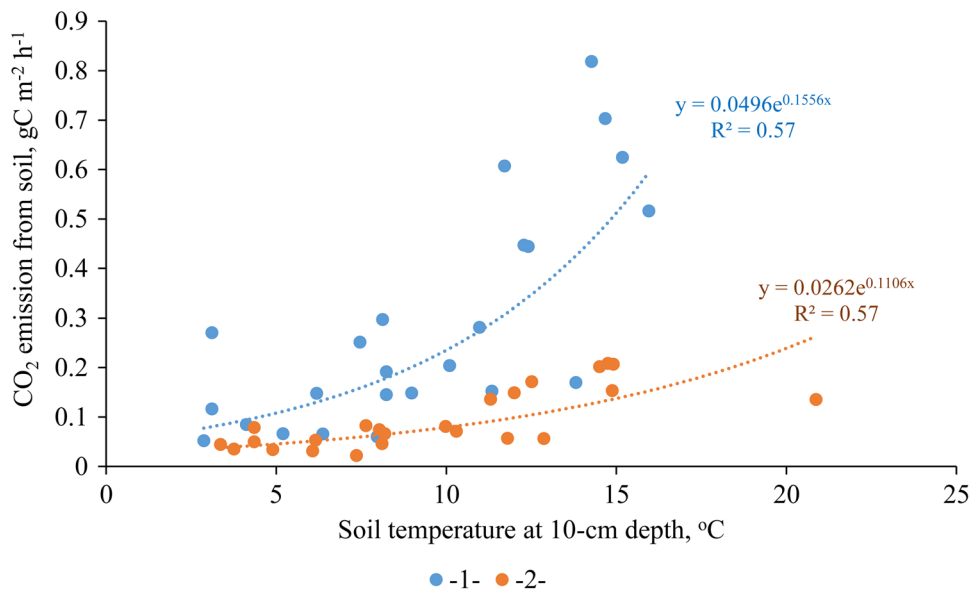


Fig. 7 The relationship between the CO₂ soil efflux and the soil temperature at a 10-cm depth from under the dry standing spruce trees and the stumps (-1-) and at the background sites (-2-) (“Taiga Log” experimental site, 2014–2018). Exponential regressions are given



in soil microbial biomass ($35.5 > 25.8 \mu\text{g C per 100 g}$ of the oven dry soil, Mann–Whitney test, $p=0.2$). However, the differences observed were too small to confirm the significant variations in the rates of soil respiration that were identified during the study.

In the summer of 2017, significant negative correlation was found between soil respiration under dry standing trees and the number of living and dead bracket fungus bodies on the stems ($r_p=-0.67, p<0.05$), their maximum age ($r_p=-0.73, p<0.05$), and wood density changes at the 1.3-m height ($r_p=-0.70, p<0.05$). Nonsignificant

negative correlations were also found for the loss of bark ($-0.35, p>0.05$) and the signs of brown rot damage ($-0.48, p>0.05$), which were obviously due to insufficient sample series. Nevertheless, the correlation was negative and significant between the average summer CO₂ soil efflux from under dry trees and the sum of all standardized variables that reflected the rate of decomposition of dry standing trees ($r_p=-0.76, p<0.05$) (Fig. 9). Hence, there was an inverse relationship between the respiration from the areas adjacent to the dry standing trees and their decomposition degree.

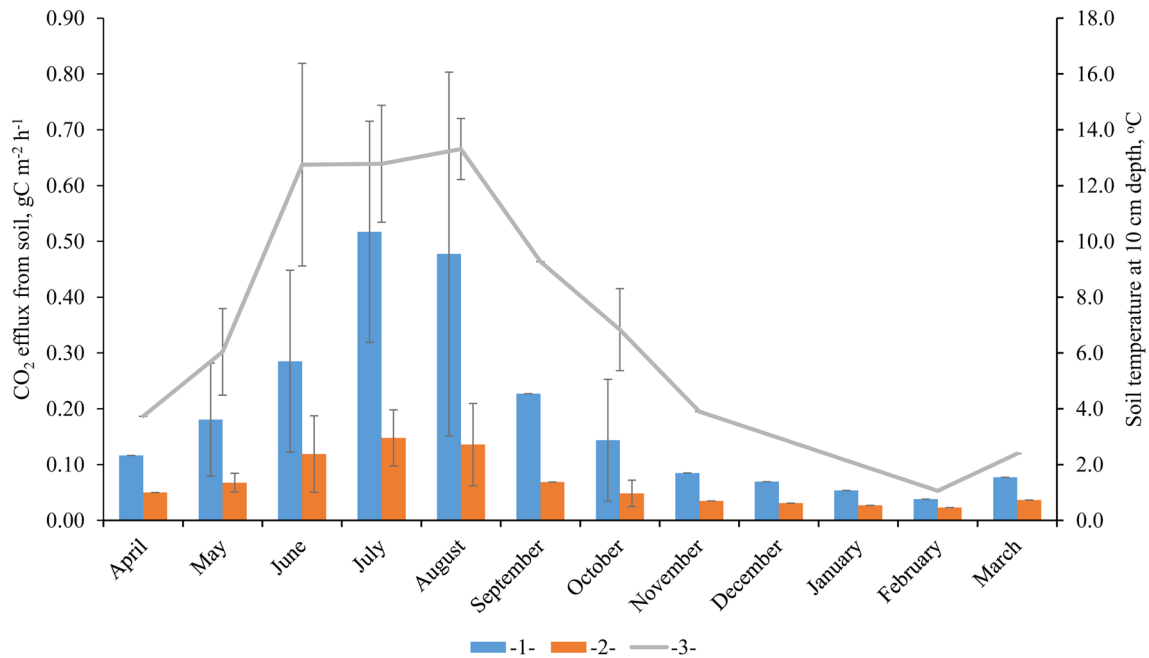


Fig. 8 The intra-annual dynamics of the CO_2 soil efflux and the soil temperature at the 10-cm depth (-3-) from 2014 to 2018. The average values and their standard errors are given ($N=1-5$). 1—the areas

adjacent to the dry standing spruce trees and the stumps and 2—the background CO_2 soil efflux

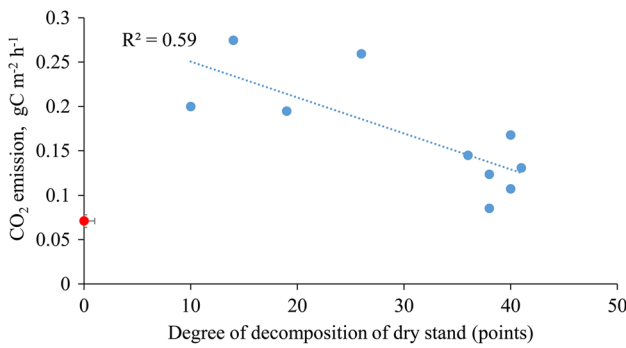


Fig. 9 The CO_2 efflux from the soil under the dry standing spruce trees and the degree of their decomposition at standardized scale points ("Taiga Log" experimental site, the summer of 2017). The single red point corresponds to the background rate of soil emission

Large-scale carbon fluxes

In 2013, the spruce forest biotope covered 58% of the transect, damaged stands and windfall trees accounted for 36%, and waterlogged depressions and bogs accounted for 6%; in 2019, this ratio changed to 35, 55 and 10%, respectively. The remote sensing data over the entire footprint showed that weakened and decaying trees comprised 8% of the stand at the experimental site in 2009, but in 2015, these trees increased to almost 30%. As decay expanded through the stand, dead trees became unprotected and fell if the wind speed exceeded 15 m s^{-1} (Karelin et al. 2017a). Satellite

and geobotanical data from July 2018 and July 2019 showed that the *EC* footprint mostly contained various types of spruce-dominated forests (70%), sedge–sphagnum birch stands (5.7%), peat bogs (7.0%) and cotton grass–sphagnum–pine stands (4.7%) (Fig. 2). The remainder of the territory (12.6%) corresponded to spruce forest damage and included dry standing trees (9%) and windfall trees (3.6%). This estimate of the moderate and weakened cover in the stand was smaller than that noted in Section "Objects and methods" because the analysis included only those areas where the living trees were completely lost.

At the initial stage of stand dieback (15 May–31 October, 2010), average horizontal wind speed was 1.76 m s^{-1} with nonsignificant variations across the eight wind sectors. This enabled the application of a single radius for all sectors in the additional analysis. The average value of the net carbon flux during that period was $-0.064 \pm 0.005 \text{ mgC m}^{-2} \text{s}^{-1}$ (carbon sink from the atmosphere; $N=6475$). The attribution of a specific carbon flux to different forest biomes was consistently checked sector by sector at different distances from the centre of the *EC* footprint using a 10-m step scale. The relationship between the net flux and the share of the territory with the dry standing trees and windfall trees was positive but nonsignificant ($r_p = +0.31, p > 0.05$). The highest correlation was found between the average net carbon flux and the share of the territory not occupied by the undamaged spruce stands (i.e. trees with intact needles) by wind sectors at a distance of 40–300 m from the centre of the footprint

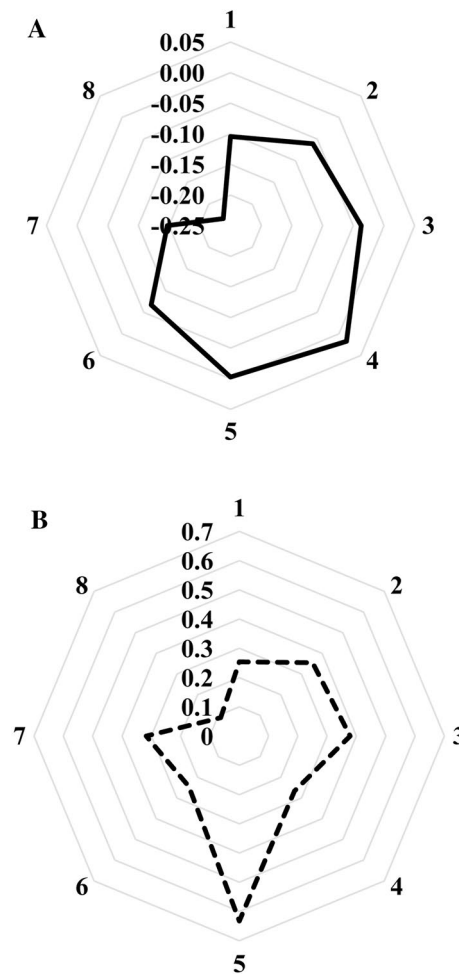


Fig. 10 The average NEE flux ($\text{mgC-CO}_2 \text{ m}^{-2} \text{ s}^{-1}$, $N=6475$) from May to October 2010 (a) and the share of the area of the undamaged spruce stands (b) by wind direction (1—north, 2—north-east ... 8—north-west) at a distance of 40–300 m from the EC tower. Negative flux values correspond to the carbon sink

(Fig. 10), but this result was also nonsignificant ($r_p = +0.66$, $p > 0.05$). The north-western sectors formed the major sink, and the south-eastern sectors were the main source of CO₂, as the areas with tree decay, peat bogs and low-density birch and pine wetlands are mainly located there.

In 2018, the average horizontal wind speed was 2.64 m s⁻¹, and there was a negligible difference between the individual sectors (paired Mann–Whitney test, $p > 0.05$) (Fig. 11). The average net CO₂ flux was $-0.023 \pm 0.002 \text{ mg C m}^{-2} \text{ s}^{-1}$ ($N=7677$). Although the ecosystem remained a net carbon sink from the atmosphere, it became significantly lower than that in 2010 (Mann–Whitney test, $p < 0.01$). The relationship between the net CO₂ flux and the share of damaged stand area increased, but remained nonsignificant ($r_p = +0.40$, $p > 0.05$). At the same time, the relationship between the net flux and the share of the area of undamaged spruce stands became significant ($r_p = +0.77$, $p = 0.026$).

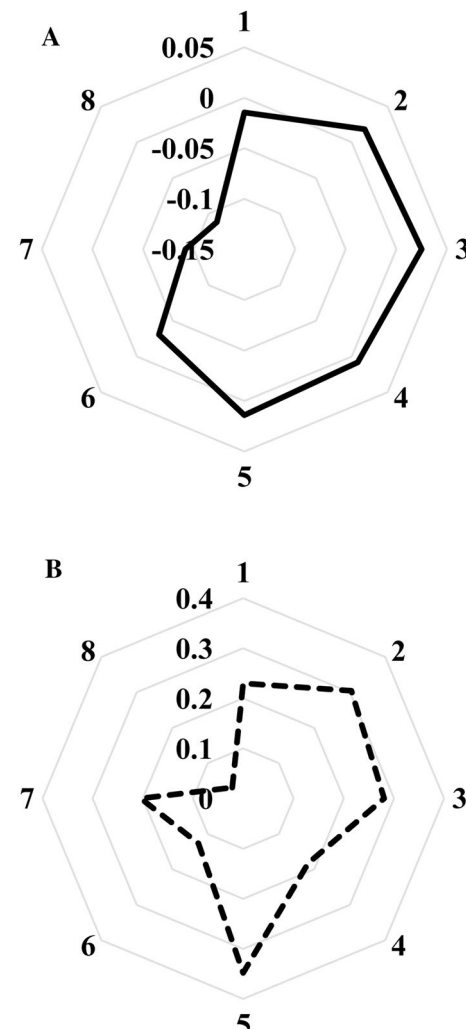


Fig. 11 The average NEE flux ($\text{mgC-CO}_2 \text{ m}^{-2} \text{ s}^{-1}$, $N=7677$) from May to October 2018 (A) and the share of the undamaged spruce stands (B) by wind direction (1—north, 2—north-east ... 8—north-west) at a distance of 30–350 m from the EC tower. Negative flux values correspond to the carbon sink

In addition, carbon sequestration of the old-growth spruce forest gradually decreased from $-300 \text{ g C m}^{-2} \text{ yr}^{-1}$ in 2010–2011 to $-95 \text{ g C m}^{-2} \text{ yr}^{-1}$ in 2018. It should be noted that from 2010 to 2018, the portion of peat bogs and birch and pine wetlands did not change within the EC footprint. At the same time, the areas with dry and windfall trees increased from 7.4 to 12.6%. Although the increment may appear negligible, it was critical to the positive correlation between the undamaged spruce forest and the net average CO₂ flux becoming significant.

A more comprehensive inventory of living and dead standing trees and the coarse woody debris pools was conducted in the main biotopes of the area in July 2019. Specific carbon stock data were obtained for the aboveground pools and were further extrapolated for the eight sectors of the EC

Fig. 12 The average NEE flux ($\text{mgC-CO}_2 \text{ m}^{-2} \text{ s}^{-1}$, $N=5206$) by eight 45° wind sectors from 1 May to 23 July 2019 vs. total dry standing spruce stock ($\text{m}^3 \text{ sector}^{-1}$), inventory (16–23 July 2019) at a distance of 30–350 m from the EC tower. Negative flux values correspond to the carbon sink. Linear regression is given

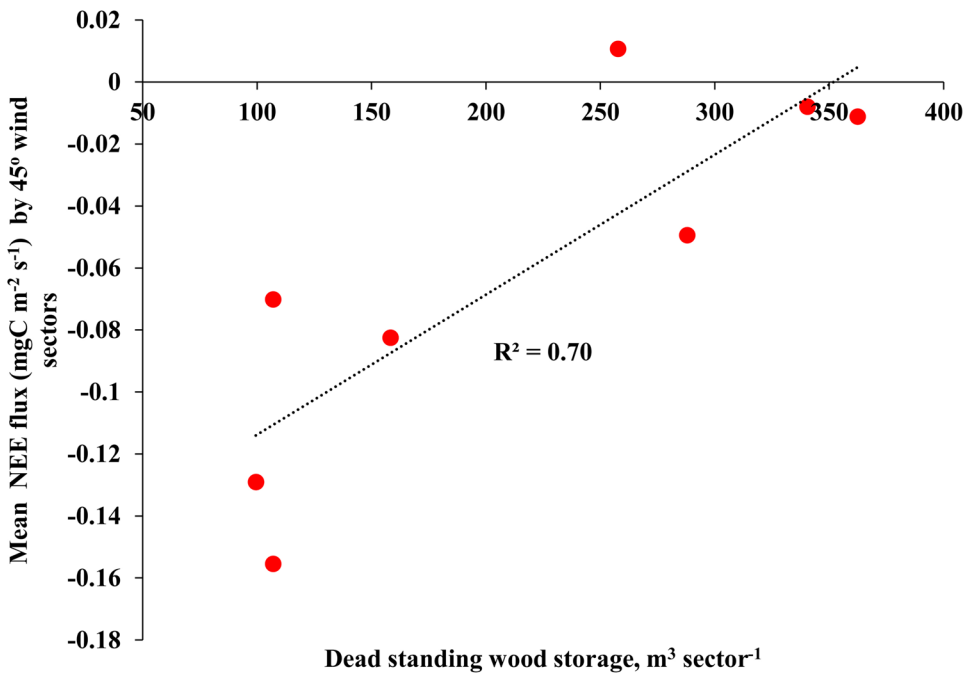
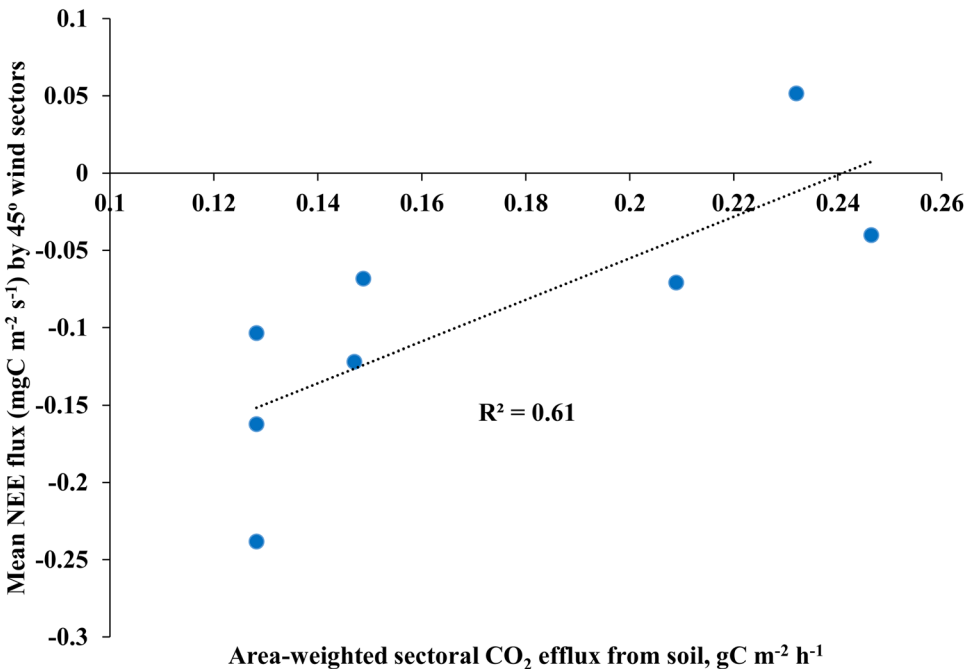


Fig. 13 The average NEE flux ($\text{mgC-CO}_2 \text{ m}^{-2} \text{ s}^{-1}$, $N=5306$) by eight 45° wind sectors from 1 May to 23 July 2019 vs. area-weighted soil CO_2 efflux ($\text{g C m}^{-2} \text{ h}^{-1}$), inventory (16–23 July 2019) at a distance of 30–350 m from the EC tower. Negative flux values correspond to the carbon sink. Linear regression is given



footprint territory. From 2009 to 2019, the coarse woody debris increased more than threefold, and the growing stock decreased from 572 to 312 $\text{m}^3 \text{ ha}^{-1}$. The results were compared with the net CO_2 flux observed during the vegetation period of 2019 (from April to July and on a monthly basis). At that time, the highest positive correlation ($r_p = +0.84$, $p < 0.01$, $N=8$) was found for all sectors between the average net CO_2 fluxes for May–July and the dry standing stocks within a 30–350-m distance from the centre of the

EC footprint (Fig. 12). In July 2019, a significant positive correlation was also found for the average weighted biotope area soil CO_2 efflux and the net CO_2 flux within a 30- to 350-m distance from the centre of the footprint (Fig. 13).

The correlation between average NEE and windfall trees by the wind sectors was positive but nonsignificant. It was the highest a 30–350-m distance in July 2019 ($r_p = +0.64$, $p > 0.05$). The relationship was inverse for the net CO_2 flux and the aboveground biomass stocks, i.e. the CO_2 removal

increased with the increasing forest phytomass. The highest correlation between these parameters was found within a 30–350-m distance from the centre of the *EC* footprint in April to July ($r_p = -0.48$, $p > 0.05$). However, this correlation was also nonsignificant, most likely due to the small sample size. Hence, dry standing-wood stock, soil respiration and coarse woody debris were the major drivers of the net CO₂ flux in the declining old-growth spruce forest, while the effect of the living spruce forest stock was less important. As the most informative area, the 30–350-m distance from the EC tower could serve as an empirical border of the footprint.

From May to October 2018, the average evapotranspiration was $0.0116 \pm 0.0002 \text{ g H}_2\text{O m}^{-2} \text{ s}^{-1}$ ($N=7677$), which was significantly lower than the $0.0142 \pm 0.0003 \text{ g H}_2\text{O m}^{-2} \text{ s}^{-1}$ ($N=6475$) in 2010 (the median test, $p = 0.027$). From May to October of 2010, the total evapotranspiration was 221 mm season⁻¹, which was 19.5% higher than that for the same period in 2018 (180 mm season⁻¹). It should be noted that despite the higher rainfall from 15 May to 31 October 2010 (462 mm) than in the same period in 2018 (367.5 mm), Selyaninov's hydrothermal coefficient was the same for both years (1.6) due to the higher temperatures in 2010 than in 2018. In addition, the reduction in evaporation corresponded to the decrease in the average net CO₂ sink from $-0.064 \text{ mg C m}^{-2} \text{ s}^{-1}$ in 2010 to $-0.023 \text{ mg C m}^{-2} \text{ s}^{-1}$ in 2018 (the Mann–Whitney test, $p < 0.01$). These differences could not be attributed to weather conditions. Most likely, the decreases in the carbon sink and evapotranspiration were the result of the reduction in primary production and the decline in old-growth spruce forest. A similar reduction in evapotranspiration was observed by Frank et al. (2014) for damaged spruce and fir forests in North America.

The field studies and modelling enabled an assessment of the major components of *ER* in the areas with spruce mortality. In the absence of a living tree canopy, the major contributors to *ER* were (i) areas adjacent to dry standing stems and stumps, (ii) coarse woody debris including dry standing trees, (iii) background soil respiration and (iv) respiration of the ground vegetation cover and undergrowth. Of these contributors, background soil respiration contributed the most to *ER*, ranging from 568.5 to 681.4 g C m⁻² yr⁻¹ ($625 \pm 20.4 \text{ g C m}^{-2} \text{ yr}^{-1}$ for $N=5$ years), with 64.8% of emissions from the noted contributors. The assessment of ground cover respiration was the least reliable because it was poorly supported with field data. However, the contribution of this source was likely second to background soil respiration. According to the chamber measurements and modeling, the contribution of herbaceous–shrubby vegetation at the initial stage of succession ranged from 105 to 191 g C m⁻² yr⁻¹ ($149 \pm 26 \text{ g C m}^{-2} \text{ yr}^{-1}$ for $N=3$ years) or 15.5%. The CO₂ release from soil under the dry standing trees and stumps unexpectedly was the next largest contributor, with

values varying from 91 to 143 g C m⁻² yr⁻¹ ($117 \pm 9.5 \text{ g C m}^{-2} \text{ yr}^{-1}$ for $N=5$ years), which was 12.1%. The smallest contribution was from the coarse woody debris including dry standing trees, which provided 46.2 to 100 g C m⁻² yr⁻¹ ($73 \pm 9.9 \text{ g C m}^{-2} \text{ yr}^{-1}$ for $N=3$ years) or 7.6%. The inter-annual variations could be explained by weather conditions (for case (ii)—mainly the air temperature) and ground vegetation growth for (iv). Finally, the *ER* in the spruce forest sites without living tree canopies was assessed as a sum of four components (i–iv) and was $964 \pm 65.8 \text{ g C m}^{-2} \text{ yr}^{-1}$ ($625 \pm 20.4 + 149 \pm 26 + 117 \pm 9.5 + 73 \pm 9.9 = 964 \pm 65.8 \text{ g C m}^{-2} \text{ yr}^{-1}$). Hence, the CO₂ sources from (ii) to (iv) comprised approximately 1/3 of the ecosystem respiration for the sites with dry trees.

We also compared the average rate of the night-time net CO₂ flux, which included the respiration of living and damaged stands over the footprint and is generally considered a minimal *ER* estimate (Valentini et al. 2000). In 2010–2011, the night-time net CO₂ flux was 936.7 g C m⁻² yr⁻¹. However, it was much higher in 2018 (1 372.8 g C m⁻² yr⁻¹). The differences between the years could also have been due to a decrease in primary production and an increase in ecosystem respiration. Consequently, tree mortality affected ecosystem respiration over the entire footprint.

Discussion

CO₂ soil efflux sources

We found that the increase in temperature increased the ratio between CO₂ soil effluxes from under dry standing trees and surrounding soil, while the increase in soil moisture decreased this ratio. These factors should be taken into account in the assessment of the spatial distribution of soil carbon fluxes in response to weather and climate variability. However, the origin of these regularities remains unclear because it is difficult to separate CO₂ production from its transport through the soil profile because soil moisture and temperature indirectly regulate respiration rates and CO₂ release to the atmosphere (Smagin 2005). Hence, pending further clarification, it would be appropriate to assume their equal contributions to CO₂ effluxes. In particular, a lower soil density is expected to promote better aeration (and consequently microbiota respiration) and facilitate gas transport via increased diffusion. Obviously, an increase in respiration can be related to microbial activity. However, under dry trees rather than at the inter-stem location, the average soil temperature at the 10-cm depth was reliably lower ($8.9 < 9.4^\circ\text{C}$, Mann–Whitney test, $p = 0.05$), and volumetric humidity was higher ($32.4 > 28.9\%$, Mann–Whitney test, $p = 0.04$). The differences may have been because litter was mostly formed from bark residues. However, that scenario would

be responsible only for a small reduction in respiration, rather than for the 2.2–3.3 times higher CO₂ release under dry standing spruce trees than in the other areas that started in 2014 and is ongoing.

Previously published estimates for the same forest site showed that the greatest CO₂ release from coarse woody debris occurred at the medium stage of wood decomposition (Safonov et al. 2012). This process follows the general pattern of wood substrate colonization by microdestructors (Harmon et al. 1986). At first, they intensively colonize the wood substrate, but later, their destructive activity and the corresponding CO₂ emissions decline due to a decrease in the quality and availability of substrate. Our data show that coarse woody debris and dry standing stems in the experimental site corresponded to the second and third stages of decomposition that were dominant in the coarse woody debris (75%), respectively. Figure 9 demonstrates significant variability in the decomposition index for dry standing trees and soil emissions from the area of the experimental plot, although the majority of trees started to decline in 2011–2012. Obviously, (i) the intensity of CO₂ release is a consequence of the destruction of belowground woody debris, represented by roots and stem bases, by xylotrophic fungi, and (ii) the destruction is highest at the medium stage of stem decomposition. The latter explains why soil emissions did not increase during the initial stages of decay of the standing trees (Fig. 9, single red dot). In addition, the transition to the final stages of decay corresponded to a decrease in the decomposition rate, which was confirmed by the dominance of highly decomposed trees currently in the plot (Fig. 9, cluster of dots on the right).

The physicochemical properties of boreal forest soils are extremely diverse and heterogeneous due to the influence of living and dead tree roots, litter and hard-to-decompose woody debris and the constant formation of pits and mounds from fallen tree stems (Kooch et al. 2015). We assume that all these controls can lead to spatial variability in CO₂ emissions from soils and, in particular, to the formation of hotspots with high CO₂ release (Martínez-García et al. 2015). Nevertheless, hotspots with long-term continuous CO₂ release capable of affecting the carbon balance of the entire community are rare and have been poorly documented. Our recent publications highlight the effect of abrupt and extended enhancements of CO₂ emissions under dry trees that died from combined attacks of bark beetles and mottled butt rot (Karelin et al. 2017a, b). Such releases are the main reason for deviations from the typical spatial distribution of the emissions observed for this forest biome. Similar hotspots of soil CO₂ emissions owing to drought-induced tree mortality events were registered after the extremely dry year (2012) in the Carpathian Mountains in Romania (Curiel Yuste et al. 2019). Four to five years after the dieback of three dominant conifer species, the emissions from under

the dead stems were 21% higher than those under the living trees. In our case, a similar amplification was much more pronounced (see also Karelin et al. 2017a, b).

Gross ecosystem fluxes and the carbon net exchange

The rates of ecosystem respiration in the damaged spruce forest are highly dependent on the coarse woody debris stocks and the recovery succession stage. The estimated respiration rate in the damaged forest ($964 \pm 65.8 \text{ g C m}^{-2} \text{ yr}^{-1}$) was not different from the eddy covariance nighttime average value in 2010–2011, when the dieback had just started and most of the stand was intact. However, in 2013, the *ER* flux model estimate was $1480 \text{ g C m}^{-2} \text{ yr}^{-1}$ for the $25 \times 40\text{-m}$ plot with the damaged spruce forest, and this value was much higher than the analogous estimates of $+922.1$ and $+970.7 \text{ g C m}^{-2} \text{ yr}^{-1}$ for the two plots with living spruce forest (Alferov et al. 2017) and our present estimate of $+964 \pm 65.8 \text{ g C m}^{-2} \text{ yr}^{-1}$.

Despite the uncertainty of the respiration estimates, it is clear that the areas of transition from living to dry standing trees and windfall trees became a long-term net carbon source. From 16.08.2010 to 15.08.2011, the initial net annual carbon budget of the footprint was equal to $-300 \text{ gC m}^{-2} \text{ yr}^{-1}$, thus functioning as a strong CO₂ sink from the atmosphere. A simple calculation shows that the net source of $+964 \text{ g C m}^{-2} \text{ yr}^{-1}$ estimated for the area of standing dry trees and windfall trees is equivalent to 12.6% of the area of the *EC* footprint, and this value reduces the overall offset of the forest site to $-140.7 \text{ g C m}^{-2} \text{ yr}^{-1}$. Further transformation into a net carbon source may occur if the dead stands increase to more than 27% of the footprint area. Most likely, this scenario has already occurred due to ongoing dieback of trees and accumulation of coarse woody debris. The recent EC measurements showed that the annual C sink decreased to $-95 \text{ g C m}^{-2} \text{ yr}^{-1}$ ($N=13,519$ of 30-min intervals). We believe that the 2018 increase in ecosystem respiration from the *EC* footprint was mostly due to progressive tree mortality in current and previous years.

CO₂ release through dry standing trees and stumps is another potential unaccounted flux. Limited information is available on this potential source, but we found a reference to emissions from pine stumps after natural fires in Spain (Martínez-García et al. 2015). In the case of post-fire events, CO₂ release through the burnt woody surface could be as high as 19% higher than the common soil flux for several years, and this area could be treated as a hotspot that was formed by alleviated gas transport through dead wood with supplementary effects of soil emissions (Martínez-García et al. 2015).

In 2007, the *Kirill* hurricane caused windfall events in old-growth spruce forests in the Austrian Alps. This is the

most relevant case of the effects of boreal forest dieback on carbon balance. In the 3rd year after the hurricane event, the windfall area became a carbon source at $405 \pm 15 \text{ g C m}^{-2}$ from May to October (Matthews et al. 2017). However, the balance remained in an almost neutral state in the next 8 years ($4 \pm 16 \text{ g C m}^{-2}$). Considering that the undisturbed forest was a carbon sink equivalent to $-415 \pm 56 \text{ g C m}^{-2}$ (Etzold et al. 2011), the authors concluded that substantial time is required for a carbon balance to be restored to its initial state. In 2008, the clear-cut of a spruce plantation established in 1916 in the north-eastern USA transformed the area into a source of $700 \text{ g C m}^{-2} \text{ yr}^{-1}$ for the first 3 years after the felling (Williams et al. 2013). A recent clear-cut in the Tver region of Russia transformed a former spruce forest into a source of $706 \pm 278 \text{ g C m}^{-2}$ during the warm period, while a similar undisturbed forest remained a minor net source of $21 \pm 278 \text{ g C m}^{-2}$, which can be considered an almost neutral state (Mamkin et al. 2019). In this scenario, the increase in carbon release intensity was the consequence of a decrease in the *GPP*, whereas ecosystem respiration for the clear-cut site was nearly the same as that for the undisturbed forest. These examples demonstrate that the actions that cause complete destruction of boreal forest stands mostly convert the area into a net source of hundreds g C yr^{-1} . In our case, the majority of forest stands remained undisturbed. This caused a notable decrease in carbon removal instead of a subsequent conversion of the area into a net carbon source. As shown by the latest satellite data (*Planet Scope* images of 10.03.20 and 26.03.20), the series of local hurricanes with wind speeds of $15\text{--}20 \text{ m s}^{-1}$ in October–December 2019 reduced the living forest cover over the footprint from 70% in July 2019 to 45.6% in March 2020. It is highly likely that the area has become the net source of carbon dioxide to the atmosphere. However, these data have not been included in the present publication, and they are the topic of our further research.

Conclusion

Within an 11-year period (2009–2019), the ongoing decay of a spruce forest did not result in an evident shift in ecosystem respiration in the areas with tree mortality compared to that in unaffected stands. This result mostly occurred based on the compensation of autotrophic respiration of living trees by heterotrophic respiration from soil under dry standing spruce trees and newly formed coarse woody debris and the respiration of plants at initial stages of succession recovery. The CO₂ hotspots adjacent to dry standing trees were the important added value for carbon emissions per area of declined stands, being almost constant during the period of our study. Their specific respiration rates were almost 60% higher than the rate of coarse woody debris. We believe that the hotspots occur under dry trees due to intensive

underground respiration of saprophytic fungi and increased gaseous release from soil.

In addition, the *EC* data showed that CO₂ removal in the spruce forest within the *EC* footprint (~40 ha) decreased from $-300 \text{ g C m}^{-2} \text{ yr}^{-1}$ in 2010–2011 to $-95 \text{ g C m}^{-2} \text{ yr}^{-1}$ in 2018. Most likely, this decrease was due to progressive damage to the stand. This result was confirmed in 2019, when strong positive correlations were found between the net CO₂ flux and dry standing tree stock and soil CO₂ efflux. Since the damage resulted in a significant decrease in evapotranspiration, we assume that the reduction in the carbon sink was due to both the decline in primary production of the tree canopy and the reduction in the area of living spruce stands.

Acknowledgements The authors are grateful to Dr. Victor A. Mukhin for valuable advice and assistance in describing fungal damage of spruce stand and to the students of the chair of *Ecology and Nature Management* of the Biology Department, Lomonosov Moscow State University, for their contribution to forest inventories and vegetation mapping.

Author contributions All authors contributed to the study conception and design. Material preparation, data collection and analysis were performed by Dmitry V. Kareljin, Dmitry G. Zamolodchikov, Arseny V. Shilkin, Sergey Yu. Popov, Anton S. Kumanyaev, Valentin O. Lopes de Gerenu, Natalia O. Tel'nova and Michael L. Gitarskiy. The manuscript was written by Dmitry V. Kareljin and Michael L. Gitarskiy, and all authors commented on it. The final version was edited and translated by Michael L. Gitarskiy. All authors read and approved the final manuscript.

Funding This research was funded by the Russian Science Foundation (grant 18-17-00178), the State Assignment AAAA-A18-118052400130-7 for the Center for Forest Ecology and Productivity of Russian Academy of Sciences (RAS), the State Assignment 0148-2019-0006 for the Institute of Geography RAS and the State Assignment AAAA-A17-117072710019-8 for “Tayphoon” Research Association of the Roshydromet (Russia).

Code availability The statistical software applied for data treatment is licensed. The licenses are the property of the affiliated authors' institutions.

Compliance with ethical standards

Conflicts of interest The authors declare that they have no conflict of interest.

Availability of data and material All data generated and analyzed during this study are included in this article and supplementary material submitted together with it.

References

- Alferov AM, Blinov VG, Gitarskiy ML, Grabar VA, Zamolodchikov DG, Zinchenko AV, Ivanova NP, Ivakhov VM, Karaban RT, Kareljin DV, Kalyuzhniy IL, Kashin FV, Konyushkov DE, Korotkov

- VN, Krovotyntsev VA, Lavrov SA, Marunich AS, Paramonova NN, Romanovskaya AA, Trunov AA, Shilkin AV, Yuzbekov AK (2017) Monitoring of the greenhouse gas fluxes in the natural ecosystems. Zamolodchikov DG, Karelín DV, Gitarskiy ML, Blinov VG (eds) Amirit, Saratov. https://downloads.igce.ru/publications/Gitarsky_M_L/Monograph_Gitarsky_M_L_et_al-60x90-new-16-10-2017.pdf (in Russian)
- Allen CD, Macalady AK, Chenchouni H et al (2010) A global overview of drought and heat-induced tree mortality reveals emerging climate change risks for forests. *For Ecol Manag* 259:660–684
- Anderson JPE, Domsch KH (1978) A physiological method for the quantitative measurement of microbial biomass in soils. *Soil Biol Biochem* 10(3):215–221
- Anderson MJ, Gorley RN, Clarke KR (2008) PERMANOVA+ for PRIMER: guide to software and statistical methods. PRIMER-E Ltd, Plymouth
- Baldocchi DD, Meyers TP (1991) Trace gas exchange above the floor of a deciduous forest: evaporation and CO₂ flux. *J Geophys Res Atmos* 96:7271–7285
- Bohn TJ, Podest E, Schroeder R, Pinto N, McDonald KC, Heimann M, Lettenmaier DP (2013) Modelling the large-scale effects of surface moisture heterogeneity on wetland carbon fluxes in the west Siberian lowland. *Biogeosciences* 10(10):6559–6576
- Bonan GB (2008) Forests and climate change: forcings, feedbacks, and the climate benefits of forests. *Science* 320:1444–1449
- Bond-Lamberty B, Thomson A (2010) Temperature-associated increases in the global soil respiration record. *Nature* 464:579–582
- Burba G (2013) Eddy covariance method for scientific, Industrial, Agricultural and Regulatory Applications, LI-COR Biosciences
- Curiel Yuste J, Flores-Rentería D, García-Angulo D, Hereş A-M, Bragă C, Petritan A-M, Petritan IC (2019) Cascading effects associated with climate-change-induced conifer mortality in mountain temperate forests result in hot-spots of soil CO₂ emissions. *Soil Biol Biochem*. <https://doi.org/10.1016/j.soilbio.2019.02.017>
- Dobor L, Hlásny T, Rammer W, Barka I, Trombík J, Pavlenka P, Šebeň V, Štěpánek P, Seidl R, (2018) Post-disturbance recovery of forest carbon in a temperate forest landscape under climate change. *Agric For Meteorol* 263:308–322
- Etzold S, Ruehr N, Zweifel R, Dobbertin M, Zingg A, Pluess P, Hässler R, Eugster W, Buchmann N (2011) The carbon balance of two contrasting mountain forest ecosystems in Switzerland: similar annual trends, but seasonal differences. *Ecosystems* 14(8):1289–1309
- Fang C, Moncrief JB, Gholz HL, Clark KL (1998) Soil CO₂ efflux and its spatial variation in a Florida slash pine plantation. *Plant Soil* 205:135–146
- Frank JM, Massman WJ, Ewers BE, Huckaby LS, Negron JF (2014) Ecosystem CO₂/H₂O fluxes are explained by hydraulically limited gas exchange during tree mortality from spruce bark beetles. *J Geophys Res G: Biogeosci* 119:1195–1215
- Gitarskiy ML, Zamolodchikov DG, Mukhin VA, Grabar VA, Diyarova DK, Ivashchenko AI (2017) Carbon fluxes from coarse woody debris in southern taiga forests of the Valdai upland. *Russ J Ecol* 48(6):539–544. <https://doi.org/10.1134/S1067413617060030>
- Gitarskiy ML, Zamolodchikov DG, Mukhin VA, Diyarova DK, Grabar VA, Karelín DV, Ivashchenko AI, Marunich AS (2020) Seasonal variations in carbon dioxide emissions during the fallen spruce trees decomposition in Southern taiga. *Russ J For Sci* 3:239–249. <https://doi.org/10.31857/s0024114820030055>
- Grabovsky VI, Zamolodchikov DG (2012) Models of estimating slash reserves according to data obtained on transects. *Russ J For Sci* 2:66–73 (in Russian)
- Han M, Shi B, Jin G (2018) Conversion of primary mixed forest into secondary broadleaved forest and coniferous plantations: Effects on temporal dynamics of soil CO₂ efflux. *CATENA* 162:157–165
- Harmon ME, Franklin JF, Swanson FJ, Sollins P, Gregory SV, Lattin JD, Anderson NH, Cline SP, Aumen NG, Sedell JR, Lienkaemper GW, CromackKJr, Cummins KW (1986) Ecology of coarse woody debris in temperate ecosystems. In: MacFadyen A, Ford ED (ed) Advances in ecological research. Inc. 15. Academic Press, Orlando, pp133–302
- Hicke JA, Allen CD, Desai AR, Dietze MC, Hall RJ, Hogg EH, Kashian DM, Moore D, Raffa KF, Sturrock RN, Vogelmann J (2012) Effects of biotic disturbances on forest carbon cycling in the United States and Canada. *Glob Change Biol* 18:7–34
- Karelín DV, Pochikalov AV, Zamolodchikov DG, Gitarskiy ML (2014) Factors of spatiotemporal variability of CO₂ fluxes from soils of southern taiga spruce forests of Valdai. *Contemp Probl Ecol* 7(7):743–751
- Karelín DV, Zamolodchikov DG, Isaev AS (2017) Unconsidered sporadic sources of carbon dioxide emission from soils in taiga forests. *Doklady Biol Sci* 475:165–168
- Karelín DV, Pochikalov AV, Zamolodchikov DG (2017b) Effect of amplification of CO₂ emission in decay areas in Valday forests. *Izvestiya Rossiiskoi Akademii Nauk. Seriya Geograficheskaya* 2:60–68. <https://doi.org/10.15356/0373-2444-2017-2-60-68> (in Russian)
- Knöhl A, Kolle O, Minayeva T, Milyukova I, Vygodskaya N, Foken T, Schulze E (2002) Carbon dioxide exchange of a Russian boreal forest after disturbance by wind throw. *Glob Change Biol* 8:231–246
- Kohout P, Charvátová M, Štursová M, Mašínová T, Tomšovský M, Baldrian P (2018) Clearcutting alters decomposition processes and initiates complex restructuring of fungal communities in soil and tree roots. *ISME J* 12:692–703
- Kooch Y, Darabi SM, Hosseini SM (2015) Effects of pits and mounds following windthrow events on soil features and greenhouse gas fluxes in a temperate forest. *Pedosphere* 25(6):853–867. [https://doi.org/10.1016/S1002-0160\(15\)30066-7](https://doi.org/10.1016/S1002-0160(15)30066-7)
- Koptzik GN, Kadulin MS, Zakharchova AI (2015) The effect of technogenic contamination on carbon dioxide emission by soils in the Kola Subarctic. *Biol Bull Rev* 5:480. <https://doi.org/10.1134/S2079086415050047>
- Köster K, Puttsepp U, Pumpanen J (2011) Comparison of soil CO₂ flux between uncleared and cleared windthrow areas in Estonia and Latvia. *For Ecol Manag* 262:65–70
- Lindauer M, Schmid HP, Grote R, Mauder M, Steinbrecher R, Wolpert B (2014) Net ecosystem exchange over a non-cleared wind-throw-disturbed upland spruce forest—Measurements and simulations. *Agric For Meteorol* 197:219–234
- Lindroth A, Lagergren F, Grelle A, Klemedtsson L, Langvall O, Westlien P, Tuulik J (2009) Storms can cause Europe-wide reduction in forest carbon sink. *Glob Change Biol* 15:346–355
- Mamkin V, Kurbatova J, Avilov V, Ivanov D, Kuricheva O, Varlagin A, Yaseneva I, Olchev A (2019) Energy and CO₂ exchange in an undisturbed spruce forest and clear-cut in the Southern Taiga. *Agric For Meteorol* 265:252–268
- Martínez-García E, López-Serrano FR, Dadi T, García-Morote FA, Andrés-Abellán M, Rubio E (2015) Carbon loss during the early decomposition stages of tree stumps in a post-wildfire Spanish black pine forest. *For Ecol Manage* 358:321–334
- Matthews B, Mayer M, Katzensteiner K, Godbold DL, Schume H (2017) Turbulent energy and carbon dioxide exchange along an early-successional windthrow chronosequence in the European Alps. *Agric For Meteorol* 232:576–594
- Morris SJ (1999) Spatial distribution of fungal and bacterial biomass in southern Ohio hardwood forest soils: fine scale variability and microscale patterns. *Soil Biol Biochem* 31:1375–1386
- Ney P, Graf A, Bogena H, DiekkrügerB DrüeC, EsserO HeinemannG, KlosterhalfenA PickK, PützT SchmidtM, VallerV VereckenH

- (2019) CO₂ fluxes before and after partial deforestation of a Central European spruce forest. *Agric For Meteorol* 274:61–74
- Pan Y, Birdsey RA, Phillips O, Jackson RB (2013) The structure, distribution, and biomass of the world's forests. *Annu Rev Ecol Evol Syst* 44:593–622
- Peters EB, Wythers KR BJB, Reich PB (2013) Influence of disturbance on temperate forest productivity. *Ecosystems* 16(1):95–110
- Qi Y, Dong Y, Jin Z, Peng Q, Xiao S, He Y (2010) Spatial heterogeneity of soil nutrients and respiration in the desertified grasslands of inner Mongolia, China. *Pedosphere* 20(5):655–665
- Safonov SS, Karelín DV, Grabar VA, Latyshev BA, Grabovskiy VI, Uvarova NE, Zamolodchikov DG, Korotkov VN, Gytarsky ML (2012) The emission of carbon from the decomposition of woody debris in the southern taiga spruce forest. *Russ J For Sci* 5:44–49 (in Russian)
- Selyaninov GT (1928) About climate agricultural estimation. *Proc Agric Meteorol* 20:165–177
- Shu S, Zhu W, Wang W, Jia M, Zhang Y, Sheng Z (2019) Effects of tree size heterogeneity on carbon sink in old forests. *For Ecol Manage* 432:637–648
- Smagin AV (2005) The soil gaseous phase. Moscow State University Publishers, Moscow (in Russian)
- Smagin AV, Dolgikh AV, Karelín DV (2016) Experimental studies and physically substantiated model of carbon dioxide emission from the exposed cultural layer of Velikii Novgorod. *Eurasian Soil Sci* 49(4):450–456
- Štúrsová M, Šnajdr J, Cajthaml T, Bárta J, Šantrůčková H, Baldrian P (2014) When the forest dies: the response of forest soil fungi to a bark beetle-induced tree dieback. *ISME J* 8:1920–1931
- Subke JA, Reichstein MM, Tenhunen JD (2003) Explaining temporal variation in soil CO₂ efflux in a mature spruce forest in southern Germany. *Soil Biol Biochem* 35(11):1467–1483
- Treifeld RF, Krainka ON, Povarov ED (2002) The method forevaluation of mass of coarse woody debris based on ground forest inventory data. Pushkino (in Russian)
- Utkin AI, Zamolodchikov DG, Gulbe TA, Gulbe YI (1996) The allometric equations for the phytomass based on the pine, spruce, birch and aspen tree data in the European part of Russia. *Russ J For Sci* 6:36–45 (in Russian)
- Utkin AI, Zamolodchikov DG, Gulbe TA, Gulbe YI, Milova OV (2005) Phytomass-dependent predictors of above-ground net primary production of plantations of the main forest-forming species of Russia. *Contemp Probl Ecol* 4:707–715
- Valentini R, Matteucci G, Dolman AJ, Schulze E-D, Rebmann C, Moors EJ, Granier A, Gross P, Jensen NO, Pilegaard K, Lindroth A, Grelle A, Bernhofer C, Grunwald T, Aubinet A, Ceulemans R, Kowalski AS, Vesala T, Rannik U, Berbigier P, Loustau D, Guömundsson J, Thorgeirsson H, Ibrom A, Morgenstern K, Clement R, Moncrieff J, Montagnani L, Minerbi S, Jarvis PG (2000) Respiration as the main determinant of carbon balance in European forests. *Nature* 404:861–865
- Warren WG, Olsen PE (1964) A line transect technique for assessing logging waste. *For Sci* 10:267–276
- Weibin L, Zhen B, Changjie J, Xinzong Z, Dexin G, AnzhiW FY, Jiabing W (2017) The influence of tree species on small scale spatial heterogeneity of soil respiration in a temperate mixed forest. *Sci Total Environ* 590–591:242–248
- Williams CA, Vanderhoof MK, Khomik M, Ghimire B (2014) Post-clearcut dynamics of carbon, water and energy exchanges in a midlatitude temperate, deciduous broadleaf forest environment. *Glob Change Biol* 20:992–1007
- Xu M, Qi Y (2001) Soil-surface CO₂ efflux and its spatial and temporal variations in a young ponderosa pine plantation in northern California. *Glob Change Biol* 7:667–677
- Zamolodchikov DG, Utkin AI, Korovin GN (2005) The conversion coefficients phytomass/volume in relation to dendrometry indices and structure of the stand. *Russ J For Sci* 6:73–81 (in Russian)
- Zaugolnova LB (2002) The methods for collection and preliminary assessment of geobotanical and demographic data: the field practical training manual. In: Gusev MB, Melekhov OP, Romanova EP (eds) The biodiversity conservation and restoration. Research and Methodological Center Publishing, Moscow, pp 59–77 (in Russian)

Publisher's Note Springer Nature remains neutral with regard to jurisdictional claims in published maps and institutional affiliations.